Instability Driven Fragmentation of Nanoscale Fractal Islands

C. Bréchignac,[1] Ph. Cahuzac,[1] F. Carlier,[1] C. Colliex,[1] J. Leroux,[1] A. Masson,[1] B. Yoon,[2] and Uzi Landman[2]

[1]*Laboratoire Aimé Cotton, C.N.R.S. Bâtiment 505, UPS, 91405 Orsay Cedex, France*

[2]*School of Physics, Georgia Institute of Technology, Atlanta, Georgia 30332-0430*

(Received 25 January 2002; published 26 April 2002)

Formation and evolution of fragmentation instabilities in fractal islands, obtained by deposition of silver clusters on graphite, are studied. The fragmentation dynamics and subsequent relaxation to the equilibrium shapes are controlled by the deposition conditions and cluster composition. Sharing common features with other materials' breakup phenomena, the fragmentation instability is governed by the length-to-width ratio of the fractal arms.

DOI: 10.1103/PhysRevLett.88.196103 PACS numbers: 68.55.Jk, 61.43.Hv, 81.16.Rf

The formation, evolution, and consequences of instabilities in materials systems have been the subject of fruitful inquiry for a long time [1–4]. These investigations have been performed in various disciplines (e.g., hydrodynamics, solid state physics, and materials science) and have been applied to systems characterized by different length scales, from the macroscopic [1–4] to the nanoscale [5] regimes. Such studies provide deep insights into fundamental issues pertaining to the interplay and balance governing the bulk and surface contributions to the energetics of materials, their morphological stability, and the relaxation dynamics in nonequilibrium complex systems. Furthermore, studies of such materials instabilities have important technological implications concerning the formation and control of materials systems of desired properties (e.g., nanojets [5], nanowires [6], thin films, and other surface supported structures).

Here we report on experimental and theoretical investigations of the development and evolution of morphological instabilities in supported fractal films, generated through the deposition of a narrow size distribution of silver clusters on a graphite substrate at room temperature [7,8]. We find that such deposited structures fragment (at ambient temperature) through a surface self-diffusion mechanism [4(b)], and consequently the mass density and its fractal dimension are conserved throughout the process. We demonstrate that the fragmentation dynamics and the relaxation to the equilibrium shape, can be controlled by the deposition conditions as well as by the composition of the incident clusters. Analysis of the fully fragmented fractal islands leads to identification of the ratio between the length and the width of the fractal branch (prior to fragmentation) as the critical parameter characterizing the instability that underlies the fragmentation. The emergence of such a characteristic parameter as well as its critical value (typically of the order of 4.5), implies that the fragmentation of surface-supported solid fractal structures studied here shares the same universality class as other instability driven fragmentation phenomena [1–4].

Under appropriate conditions, films grown through the deposition of preformed clusters exhibit a nonequilibrium fractal pattern [7,9]. The fractal shape of the supported islands is a consequence of the diffusion limited aggregation (DLA) mechanism [10], and studies pertaining to the morphological stability of the films provide valuable information about the intrinsic properties of these nonequilibrium objects. However, experimental reports about fractal stability are scarce [11,12]. In these experiments, fractal islands relax upon thermal annealing into more compact forms and no fragmentation has been observed. Nevertheless, numerical simulations predicted a late (post-growth) fragmentation stage, with periphery diffusion as the dominant mass transport mechanism [13–16]. Our experiments provide evidence for fractal fragmentation within a time scale that depends strongly on the fractal branch width and on the surface self-diffusion coefficient. The surface diffusion current is proportional to the local gradient of the fractal branch curvature [[4,14,17], and Eq. (1) below].

Gas-phase neutral silver clusters, produced by a gas-aggregation cluster source [7], are deposited at low impact energy (0.05 eV/atom), on a room temperature cleaved graphite surface maintained at a high vacuum (10^{-9} torr). The neutral cluster size distribution is measured by a time-of-flight mass spectrometer. The distribution is characterized by a Gaussian with a peak at 150 atoms (i.e., clusters with a mean diameter of 2 nm) and a full width of half-maximum corresponding typically to 20% of the mean diameter value. A crystal quartz microbalance measures the flux of the incident neutral clusters (of the order of 10^{10} clusters/cm^2 s, with deposition times between 1 to 30 min). Since the per-atom kinetic energy of the incident clusters is very low compared with their binding energy (1.2 eV/atom) the clusters migrate on the surface as a whole and grow into islands [7] which can continue to evolve past the formation stage. The prepared samples were either transferred in air and imaged in a scanning electron microscope (SEM), or transferred into high vacuum and imaged with a noncontact atomic force microscope (AFM). The similarity between the images obtained in both cases, shows that the transfer in air does not affect the island morphologies. We verified by X-ray photoemission spectroscopy that further evolution of the deposited islands after transfer in air is hindered by surface oxidation. Therefore, we can define an observation time window

 © 2002 The American Physical Society

(OTW) that starts from the beginning of the deposition and ends when the sample is exposed to air (typical observation time is of the order of 1 h).

In previous studies we have shown that the morphologies of islands generated by cluster deposition are the consequence of the interplay between the coalescence time (that is, the time for an added cluster to merge into the island) and the aggregation time interval t_a, which is the time lapse between two successive arrivals of clusters to the island [7]. When the coalescence time exceeds t_a a ramified fractal shape develops with a constant branch width l_0. This value depends on the size of the incident clusters, on the flux, and—to some extent—on the deposition time at high coverage. l_0 decreases for larger clusters and/or higher flux, and it increases with time at high coverage [7].

In the first set of experiments we illustrate the effect of the fractal branch width on the fragmentation propensity. Figures 1a and 1b show SEM images of typical individual Ag fractal islands (with the fractal dimension [10] $D_f = 1.7$). The two coverages that we show were obtained by carrying out the deposition for 7 min, and subsequently blocking half of the substrate by a mask and continuing the deposition onto the unmasked half for an additional interval of 20 min. The islands shown in Figs. 1a and 1b have approximately the same global size ($L \sim 1$ μm). At large coverage (6 ML, unmasked part), the grown islands are characterized by thick branches ($l_0 = 25$ nm, see Fig. 1a) and they are not fragmented, except occasionally at the center of the island. On the other hand, at small coverage (2 ML, masked part) the fractal islands show thinner branches ($l_0 = 15$ nm, see Fig. 1b) and, within our OTW, they exhibit fragmentation throughout the island. Treating the fractal as a set of consecutive bars and focusing on the main branches (defined as the longest continuous quasilinear segments), the histograms on the side of the images in Fig. 1 depict the number distributions of bars as a function of the bar length, showing a shift to smaller length as the branch width decreases. For the system shown in Fig. 1b the fragments have not reached their equilibrium spherical shape. The nonobservability of fragmentation in Fig. 1a and the incomplete fragmentation in Fig. 1b, are consequences of our OTW value and the slow room-temperature fragmentation kinetics (see below).

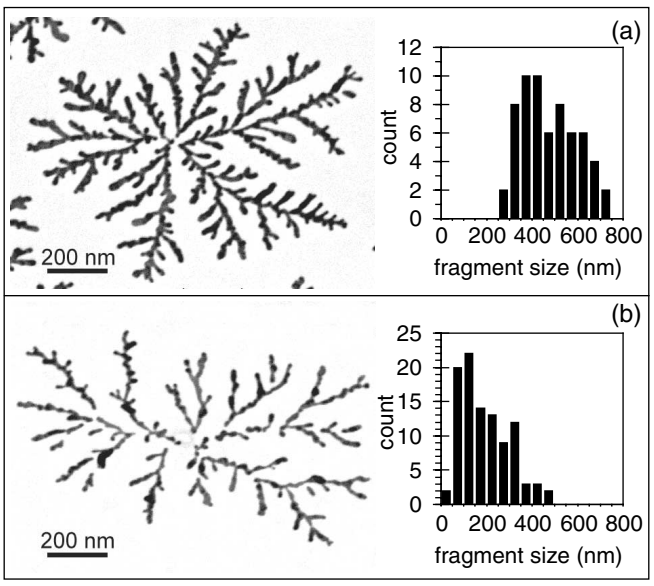

FIG. 1. SEM images of silver fractal islands and histograms of their branch-lengths (right insets), obtained from deposition of Ag_{150} clusters on graphite, for two different coverages: (a) 6 ML, and (b) 2 ML.

In a second set of experiments we vary the composition of the incident clusters by adding trace amounts of oxygen and water during the silver cluster formation stage (i.e., before deposition). Figure 2 shows SEM images of (multi-island) fractal films obtained, for the same coverage, through deposition of pure silver clusters (Fig. 2a), and via deposition of clusters with varying trace amount of oxygen (Figs. 2b and 2c). An overall characterization of the deposited film can be obtained through a 2D Voronoi polygon construction [18], with each Voronoi cell being associated with a single island. The density of Voronoi polygons is

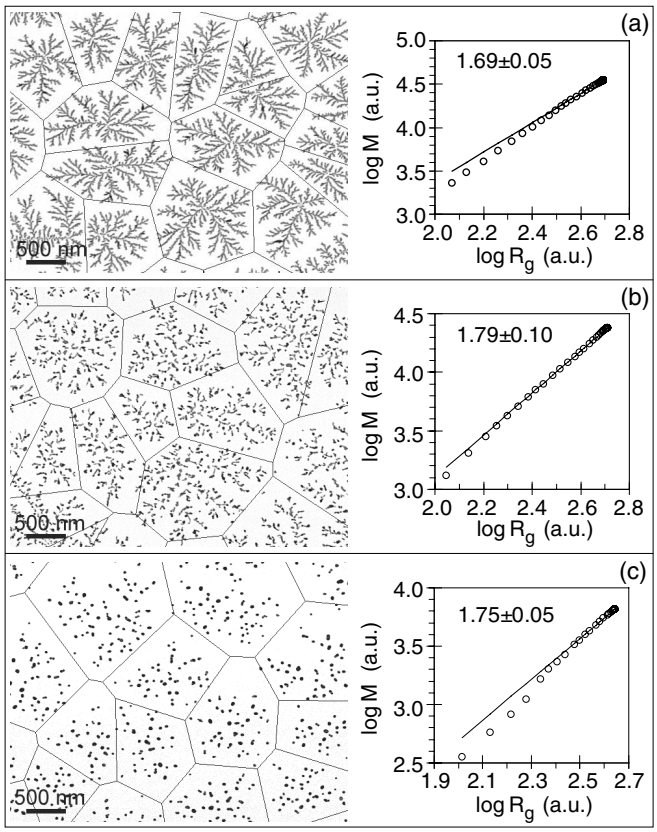

FIG. 2. Influence of an impurity in the incident clusters on the stability of the fractal islands. The SEM image in (a) corresponds to deposition of Ag_{100} clusters and those in (b) and (c) correspond to deposition of such clusters but with 0.5% and 1% oxygen impurity, respectively. In all the images a Voronoi polygon construction is superimposed. On the right of the images analysis [19] of the fractal dimension is displayed, and the asymptotic values are given.

determined by the nucleation sites (most likely defects) on the graphite surface (10^8 sites/cm^2). As aforementioned, islands obtained from deposition of pure clusters under the above conditions do not undergo fragmentation (Fig. 2a), whereas those resulting from clusters with a variable trace amount of oxygen are fragmented. The measured density of fragments is the same for the data shown in Figs. 2b and 2c, and in the latter the shape relaxation of the fragments has been completed (resulting in a spherical shape). Remarkably, rather similar asymptotic values of the mass fractal dimension [11,19] ($D_f = 1.70 \pm 0.10$, see right panels in Figs. 2a–2c) were determined for both the pure and impurity-containing cluster depositions.

From the above observation of a common fractal dimension, the growth of a continuous fractal island should precede its subsequent fragmentation into many pieces. The fragmentation process was explored through examination of the correlation function between the fragments belonging to a given island. Such an analysis (performed for numerous islands) reveals a nearly constant nearest-neighbor distance λ between fragments belonging to the same fractal branch. The histogram of the nearest-neighbor distance peaks at $\lambda = 75 \pm 10$ nm. From the size distribution of the fragments we deduced a mean fragment diameter $2R = 30 \pm 3$ nm. Treating the fractal as a set of uniform cylindrical branches, the width l_0 of a branch that would have existed prior to fragmentation can be estimated from the conservation of mass, i.e., $16R^3 = 3\lambda l_0^2$. The above considerations lead to a ratio $\lambda/l_0 = 4.8$. This value is in good agreement with that obtained from linear stability analysis, yielding an optimal wavelength of $4.443 l_0$ [4(c)] for fragmentation of a solid cylinder induced by a capillary instability (through a surface self-diffusion mechanism), and interestingly it is close to the value predicted by Rayleigh for breakup of a cylindrical column of an inviscid liquid [1].

To further investigate the growth and the breakup mechanism we performed simulations [20] of the (axial) growth of a material with a 3D cylindrical symmetry, by adding spherical clusters to each side of a cylindrical structure (lying along the z axis) at an aggregation time interval t_a. The evolution of the shape of the axisymmetric material structure [4(b)] is described by

$$\frac{\partial h}{\partial t} = \frac{B}{\rho}\frac{\partial}{\partial s}\left(\rho\frac{\partial \kappa}{\partial s}\right). \quad (1)$$

Here $\partial h/\partial t$ and s are, respectively, the local transversal displacement per unit time and the curvilinear coordinate of the contour of the material structure on the ρ-z plane of the cylindrical coordinate system (ρ is the local radius of the cylinder along the z axis). κ is the local curvature expressed as $\kappa = \kappa_1 + \kappa_2$, where κ_1 and κ_2 are the curvatures defined in the ρ-z plane and in the plane normal to that which is tangent to the surface of the material structure, respectively. The fourth-order diffusion constant B [4] is given by $B = D_s \gamma \Omega^2 S_0/k_B T$ where D_s is the surface self-diffusion coefficient, γ is the surface tension, Ω is the atomic volume, and S_0 the number of atoms per unit surface area. The length and time units (tu) are selected by setting both the diameter of the incident spherical clusters, and the value of B, to unity.

For a constant aggregation time interval t_a an elongated cylinder of nearly constant width, with semispherical caps at both ends, develops at the early growth stage. When the length of the structure exceeds a critical value an instability develops, resulting in fragmentation into a string of equidistant spheres (in agreement with the 2D simulations in Ref. [14]).

To model low-frequency experimental fluctuations of the cluster source, the flux of the incident clusters is varied in the simulations during growth. Typical results of such a simulation are shown in Fig. 3. In this particular simulation we used an aggregation time $t_a = 0.1$ tu for an initial period of 22 tu, followed by a period of 5 tu during which t_a was reduced to a value of 0.09 tu, and subsequently t_a was restored to its original value. At the early stage ($t < 20$ tu), an elongated capped cylindrical shape of nearly constant width develops. As a result of the above flux fluctuation the cylinder develops a local perturbation of its width which culminates in fragmentation at

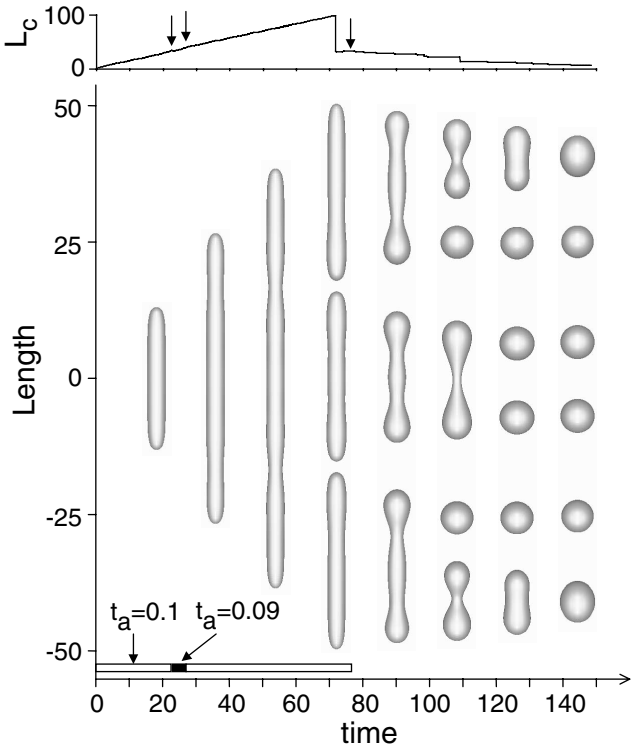

FIG. 3. Results from 3D simulations, whose procedure is described in the text. In the bottom panel the shape of the evolving cylindrical structure and fragmentation events are depicted versus time. In the upper panel the length of the longest continuous part of the cylindrical structure (i.e., the intact length) is plotted versus the simulation time; each fragmentation event is signaled by the appearance of a sawtooth shaped discontinuity, and arrows indicate a change in the clusters deposition flux. The addition of clusters is stopped for $t > 78$ tu (rightmost arrow). The length and time units are scaled as described in the text.

$t = 72$ tu. At $t = 76$ tu we stopped the addition of clusters. Subsequent evolution involves the development of morphological instabilities that lead to complete fragmentation into a string of spheres, which are not rigorously equidistant. It is of interest to remark on the evolution of the three fragments for $t > 90$ tu. We observe that while eventually all three underwent binary fragmentation, that of the middle one is mass-symmetric and those of the two end ones are asymmetric. In fact, the morphological instability of the two endmost pieces (see the peanut shapes at $t = 110$ tu) did not achieve the critical length-to-width ratio and the process culminated in relaxation into a larger-in-size spherical shape. Repeating the simulation for several arbitrary temporal fluctuations, one obtains a distribution of distances λ between neighboring spherical fragments, peaking at a value of $4.5l_0$, where l_0 is the mean diameter of the cylindrical structure (prior to fragmentation), in agreement with the experimental histograms.

Underlying the evolution of a morphological instability of an elongated solid 3D material structure is the dependence of the surface diffusion rate on the local curvature. A linear stability analysis [4(c)] of Eq. (1), limited to a small axisymmetric disturbance (with wave vector k) of the cylinder's radius, gives for the fastest growing disturbance $k^2\rho_0^2 = 0.5$, where ρ_0 is the radius of the unperturbed uniform cylinder; i.e., an optimal instability wavelength $\lambda_c = 2^{1/2}2\pi\rho_0 \simeq 4.443l_0$. This value of λ_c/l_0 is very close to the aforementioned simulated value of $4.5l_0$. We remark that within linear stability analysis, such instability does not develop for a 2D system.

From the measured mean radius of the relaxed fractal fragments (Fig. 2c), together with mass conservation, we conclude that both the fragmented and unfragmented fractal islands are 3D in nature, with a wetting angle in the vicinity of $\pi/2$ [21]. The disturbance which may culminate in fragmentation can be either of thermal origin or caused by substrate induced stresses, and the relevant time scale for fragmentation involving surface self-diffusion is $\tau = l_0^4/B$. This implies that the kinetics of fragmentation is influenced by l_0 and/or B. Figure 1 demonstrates the influence of l_0. Using parameters for pure silver [22,23] we estimate at 300 K, $\tau(l_0 = 25\ \text{nm}) = 2300$ s and $\tau(l_0 = 15\ \text{nm}) = 300$ s. Consequently for a typical 2000 s OTW used by us, observation of room-temperature fragmentation is (kinetically) unlikely for the thicker branches (Fig. 1a), while it should be readily observed (at least partial fragmentation) for the thinner ones (Fig. 1b). Figures 2b and 2c depict complete fragmentation within the same OTW, showing evidence for a faster fragmentation kinetics (i.e., decrease of τ) with increasing trace amounts of oxygen in the incident clusters.

In summary, we found via experiments and theoretical analysis, that the room-temperature fragmentation instability of fractal islands formed through the deposition of silver clusters on graphite, is governed by the ratio of the length to the width of the fractal arms; such length-to-width control parameter is a common feature in many instability phenomena [1–5]. In particular, the wavelength of the fastest growing instability is determined by this critical ratio (having a value of ~4.5), and the actual observability of fragmentation depends on the fragmentation kinetic, involving surface self-diffusion, and thus on the experimental OTW. The fragmentation dynamics and the relaxation to the equilibrium shapes can be controlled by the deposition conditions (including size selection of the incident clusters) as well as by the composition of the incident clusters. Technological implications may include issues pertaining to the growth of surface-supported elongated structures (nanowires), and the self-organization of structures made of supported nanoparticles with well-defined sizes and interparticle spacing.

This research is supported by CNRS and the U.S. DOE (Grant No. FG05-86ER-45234). Computations were performed at the GIT Center for Computational Materials Science.

[1] J. W. S. Rayleigh, Proc. London Math. Soc. **10**, 4 (1879).
[2] S. Chandrasekhar, *Hydrodynamics and Hydrodynamic Stability* (Oxford University, New York, 1961).
[3] J. Eggers, Rev. Mod. Phys. **69**, 865 (1997).
[4] (a) W. W. Mullins, J. Appl. Phys. **28**, 333 (1957); (b) F. A. Nichols and W. W. Mullins, J. Appl. Phys. **36**, 1826 (1965); (c) F. A. Nichols and W. W. Mullins, Trans. Metall. Soc. AIME **233**, 1840 (1965).
[5] M. Moseler and U. Landman, Science **289**, 1165 (2000).
[6] *Nanowires,* edited by P. Serena and N. Garcia (Kluwer, Dordrecht, 1997).
[7] B. Yoon *et al.,* Surf. Sci. **443**, 76 (1999).
[8] I. M. Goldby *et al.,* Appl. Phys. Lett. **69**, 2819 (1996).
[9] P. Jensen, Rev. Mod. Phys. **71**, 1695 (1999).
[10] T. A. Witten and L. M. Sander, Phys. Rev. Lett. **47**, 1400 (1981).
[11] R. Q. Hwang *et al.,* Phys. Rev. Lett. **67**, 3279 (1991).
[12] H. Röder *et al.,* Nature (London) **366**, 141 (1993).
[13] T. Irisawa *et al.,* Europhys. Lett. **30**, 139 (1995).
[14] R. Thouy *et al.,* Phys. Rev. B **56**, 5321 (1997).
[15] R. Sempéré *et al.,* Phys. Rev. Lett. **71**, 3307 (1993).
[16] M. Conti *et al.,* Phys. Rev. Lett. **80**, 4693 (1998).
[17] J. Eggers, Phys. Rev. Lett. **80**, 2634 (1998).
[18] P. A. Mulheran and J. A. Blackman, Philos. Mag. Lett. **72**, 55 (1995).
[19] The asymptotic mass fractal dimension was measured for large R_g by using the power law relation between the mass M and the gyration radius R_g.
[20] The numerical method that we used is a 3D extension of the 2D simulation described in Ref. [14]. Moreover, in Ref. [14] only fragmentation after growth was simulated.
[21] M. S. McCallum *et al.,* J. Appl. Phys. **79**, 7604 (1996).
[22] C. R. Stoldt *et al.,* Phys. Rev. Lett. **81**, 2950 (1998).
[23] K. Akamatsu *et al.,* J. Phys. Chem. B **104**, 10 168 (2000).